Parameter Sensitivity Analysis to Improve Material Design for Novel Zn-MnO_2 Batteries with Ionic Liquid Electrolytes

Zachary T. Gima & Bernard J. Kim
CE 295: Spring 2016

***Abstract*—Battery design at the materials level is often an inefficient process that requires many iterations and significant development costs. To improve the design process, parameter sensitivity analysis can be performed to provide battery materials scientists with better design intiution. A parameter sensitivity analysis was developed for electrode parameters by adapting the single particle model (SPM) for a Zn-MnO_2 chemistry. Parameters of interest included particle radius and electrode thickness. The parameter sensitivity analysis determined the relative sensitivity of the battery's output voltage to these aforementioned parameters as well as their linear dependence on one another.**

I. Introduction

A. Motivation & Background

The Advanced Manufacturing for Energy lab at UC Berkeley is developing a printable, secondary Zn-MnO_2 battery for Internet of Things (IoT) and grid-scale energy storage applications (Figure 1). The battery utilizes an ionic liquid electrolyte that enables facile recharging of zinc and could potentially lead to displacement of lithium-based systems in applications where safety and cost considerations are paramount. Specifically, applications involving sensors for food or wearables would significantly benefit from a safer and less hazardous energy storage system.

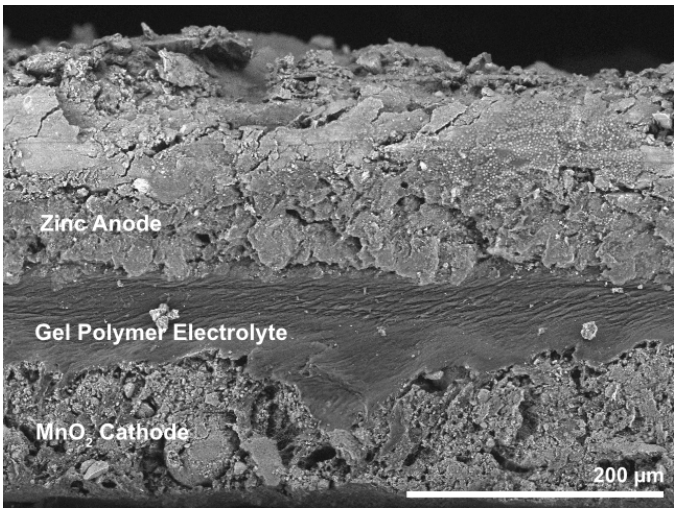

Fig. 1. Cross section SEM of Zn-MnO_2 battery developed by Advanced Manufacturing for Energy lab. The distinction between electrode and electrolyte layers is clearly visible, along with some individual particles.

Zachary T. Gima and Bernard J. Kim are with Mechanical Engineering, University of Californa, Berkeley, CA 94720, USA.
Email: {ztakeo, bernard.kim}@berkeley.edu

This class of zinc-based secondary batteries with ionic liquid electrolytes is not yet well understood or characterized. Because this research is relatively recent, there exists much room for improvement beyond proof-of-concept performance [1]. In order to streamline experimental design, we desire a model that can parameterize controllable battery characteristics (e.g. geometry, composition, etc.) and predict resulting system performance. Specifically, this model will inform key manufacturing decisions in order to best improve the battery's output voltage. Devices for IoT demand certain voltage minimums in order to operate electronic components, and improving the battery's system voltage will help the system meet this minimum over a larger range of charge.

This study utilizes the single particle model (SPM) [2], [3] for its simplicity over more sophisticated models (such as Doyle-Fuller-Newman [4]). The model is accurate for low C-rates, which are typical of our battery. The SPM models each electrode as a single porous spherical particle and assumes constant ion concentration within the electrolyte with respect to space and time [2], [3]. When applied to our battery, this model will help optimize electrode composition in order to further improve overall performance.

B. Relevant Literature

Lithium-ion batteries have emerged as the battery of choice for portable electronics, as well as in vehicular and aerospace applications [5], [6]. In order to fully utilize the capability of these batteries, a battery management system must be deployed with the battery to ensure safe and optimal operation for a given application [5]. More sophisticated versions of these management systems employ an electrochemical model describing the battery's dynamics to monitor key performance parameters such as state-of-charge and internal resistance [7]. However, if the system's dynamics are not well understood, then the model may provide insight into the battery's behavior under certain load conditions.

The single particle model (SPM) was derived from a simplified version of the complete Doyle-Fuller-Newman model [3], [4] and has been widely utilized to model and understand lithium-ion batteries [2], [3], [7]. While the assumptions the SPM makes limit the model's applicability to scenarios with low C-rates or negligible electrolyte dynamics, its simplicity and ease of solving compared to more rigorous models [4] makes it an attractive tool, especially for more fundamental analyses of electrochemical dynamics.

The Zn-MnO_2 battery of interest shares properties with previously modeled intercalation lithium-ion batteries that

make the SPM suitable to modeling this system. It has been determined that the main mechanism for charge storage in this system is with intercalation of Zn^{2+} ions into the MnO_2 cathode [8]. Furthermore, the electrolyte-agnostic assumptions of the SPM also prove to be beneficial as this battery utilizes an ionic liquid electrolyte whose solvent behavior differs significantly from traditional aqueous electrolytes [9]. The Zn-MnO_2 battery is also being cycled at low C-rates, further agreeing with this assumption [10]. By adapting the SPM to this Zn-MnO_2 system, we hope to leverage parameter sensitivity analysis on the resulting model parameters to optimize controllable geometric and compositional factors to better understand and improve the system.

C. Focus of this Study

This study will utilize the SPM to model the zinc-based battery in order to perform parameter sensitivity analysis of the battery's output voltage to particle radius and electrode thickness. The results will be used to directly modify electrode geometries and compositions in physical experiments to better tailor performance outputs for IoT demands.

II. Technical Description

This study utilizes a reduced electrochemical battery model, the SPM. This model approximates each electrode of the battery as collections of uniform particles. The dynamics of one particle at each electrode are studied and then scaled up to reflect the volume of the entire electrode. This approximation results from assuming that the concentration of insertion ions in the electrolyte phase remains constant in space and time and also that the entirety of the electrode evenly contributes to the total cell dynamics. The first assumption is reasonably valid for batteries charged and discharged at low C-rates. See Figure 2 for a graphical representation of the SPM.

For clarity, Table I provides definitions for all parameters related to the SPM that follow.

A. Single Particle Model

Specifically, the SPM results from applying the above simplifying assumptions to the more complex DFN model. The partial differential equations which therefore define the SPM come directly out of Fick's Second Law of Diffusion in spherical coordinates for symmetric, 1-D diffusion at each electrode (1)-(4). These PDEs describe the dynamics of the insertion ions in the solid phase.

$$\frac{\partial c_s^-}{\partial t}(r,t) = D_s^- \left[\frac{2}{r}\frac{\partial c_s^-}{\partial r}(r,t) + \frac{\partial^2 c_s^-}{\partial r^2}\right] \quad (1)$$

$$\frac{\partial c_s^+}{\partial t}(r,t) = D_s^+ \left[\frac{2}{r}\frac{\partial c_s^+}{\partial r}(r,t) + \frac{\partial^2 c_s^+}{\partial r^2}\right] \quad (2)$$

$$\frac{\partial c_s^-}{\partial r}(0,t) = 0, \quad \frac{\partial c_s^-}{\partial r}(R_s^-,t) = -\frac{I(t)}{D_s^- Fa^- AL^-} \quad (3)$$

$$\frac{\partial c_s^+}{\partial r}(0,t) = 0, \quad \frac{\partial c_s^+}{\partial r}(R_s^+,t) = \frac{I(t)}{D_s^+ Fa^+ AL^+} \quad (4)$$

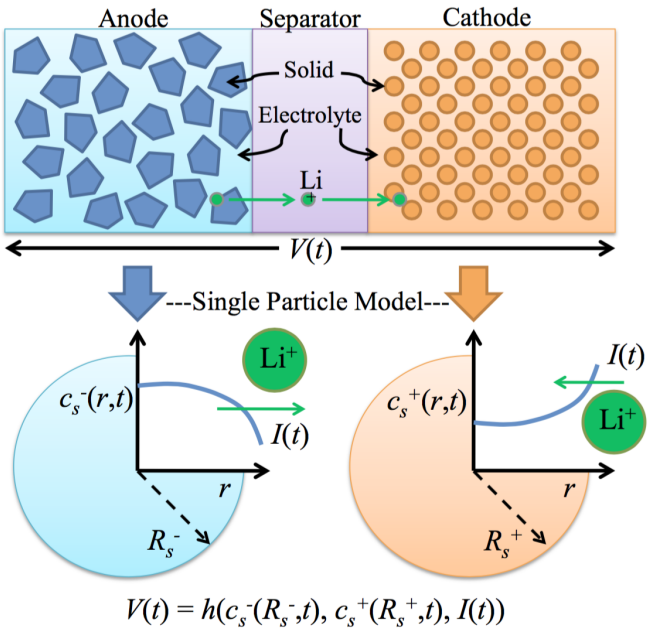

Fig. 2. Graphic representation of the SPM [3]. The electrodes are each represented as single porous spherical particles. This results from assuming electrolyte concentration remains constant in space and time.

TABLE I
Single Particle Model Parameter Definitions

Symbol	Description	SI Units
A	Cell cross sectional area	m^2
a^j	Specific interfacial surface area	m^2/m^3
c_s^j	Concentration in solid phase	mol/m^3
c_{ss}^j	Concentration at particle surface	mol/m^3
$c_{s,max}^j$	Max concentration in solid phase	mol/m^3
D_s^j	Diffusion coefficient in solid phase	m^2/m^3
F	Faraday's constant	C/mol
I	Input current	A
i_0^j	Exchange current density	V
j	Positive (+) or negative (-) electrode	-
L^j	Electrode thickness	m
R	Universal gas constant	J/mol-K
R_f	Lumped current collector resistance	Ω
R_s^j	Particle radius	m
r	Radial coordinate	m or m/m
T	Cell temperature	T
t	Time	sec or sec/sec
U^j	Equilibrium potential	V
V	Output voltage	V
α^j	Anodic/cathodic transfer coefficient	-

The Neumann boundary conditions (3) and (4) at the surfaces of the electrodes ($r = R_s^{\pm}$) proportionally relate the flux entering or exiting the electrode to the input current, $I(t)$. The boundary conditions at the center of the electrodes ($r = 0$) are required for well-posedness and spherical symmetry.

The system output is the cell voltage and is governed by a combination of Butler-Volmer kinetics, electrode thermodynamics, electrode OCP, and internal resistance (5).

$$V(t) = \frac{RT}{\alpha F}\sinh^{-1}\left(\frac{I(t)}{2a^+AL^+i_0^+\left(c_{ss}^+(t)\right)}\right) - \frac{RT}{\alpha F}\sinh^{-1}\left(\frac{I(t)}{2a^-AL^-i_0^-\left(c_{ss}^-(t)\right)}\right) + U^+\left(c_{ss}^+(t)\right) - U^-\left(c_{ss}^-(t)\right) + R_f I(t) \quad (5)$$

The exchange current density i_0^j and solid electrolyte surface concentration c_{ss}^j are described by (6) and (7). It should be noted that c_{ss}^j simply describes the solid concentration of each electrode at the boundary of the spatial dimension, *i.e.* $c_{ss}^j(t) = c_s^j(R_s^j,t)$.

$$i_0^j\left(c_{ss}^j\right) = k^j\sqrt{c_e^0 c_{ss}^j(t)\left(c_{s,max}^j - c_{ss}^j(t)\right)} \quad (6)$$

$$c_{ss}^j(t) = c_s^j\left(R_s^j,t\right), \quad j\in\{+,-\} \quad (7)$$

The full system plant is presented graphically in Figure 3.

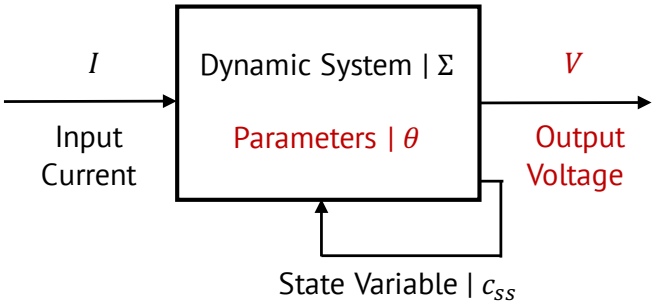

Fig. 3. Block diagram of system plant with input $I(t)$ and output $V(t)$.

B. SPM Normalization

The SPM equations (1)-(4) can be normalized in both time and space in order to facilitate the sensitivity analysis, as will be clarified later. This normalization is carried out by scaling the radial r and time t coordinates by the particle radius and characteristic diffusion time respectively (8).

$$\bar{r} = \frac{r}{R_s^-}, \qquad \bar{t} = \frac{D_s^-}{\left(R_s^-\right)^2}t \quad (8)$$

Applying this normalization to the system equations (1)-(4) yields the following modified PDEs and boundary conditions (9)-(12).

$$\frac{\partial c_s^-}{\partial \bar{t}}(\bar{r},\bar{t}) = \frac{2}{\bar{r}}\frac{\partial c_s^-}{\partial \bar{r}}(\bar{r},\bar{t}) + \frac{\partial^2 c_s^-}{\partial \bar{r}^2} \quad (9)$$

$$\frac{\partial c_s^+}{\partial \bar{t}}(\bar{r},\bar{t}) = \frac{2}{\bar{r}}\frac{\partial c_s^+}{\partial \bar{r}}(\bar{r},\bar{t}) + \frac{\partial^2 c_s^+}{\partial \bar{r}^2} \quad (10)$$

$$\frac{\partial c_s^-}{\partial \bar{r}}(0,\bar{t}) = 0, \quad \frac{\partial c_s^-}{\partial \bar{r}}(1,\bar{t}) = -\frac{R_s^- I(\bar{t})}{D_s^- Fa^- AL^-} \quad (11)$$

$$\frac{\partial c_s^+}{\partial \bar{r}}(0,\bar{t}) = 0, \quad \frac{\partial c_s^+}{\partial \bar{r}}(1,\bar{t}) = \frac{R_s^- I(\bar{t})}{D_s^+ Fa^+ AL^+} \quad (12)$$

The notable change is that the particle radius, $R_s^\pm$ now appears explicitly in the boundary condition after normalization.

Henceforth, the bars above r and t will be dropped for clarity and brevity.

C. Sensitivity Equations

Next, we derive the sensitivity equations. We want to study the influence of the parameters with respect to the system output, not the states. That is, for a given change in our parameters, we want to study how the system's output voltage reacts (13).

$$\frac{\partial y}{\partial \theta} = \frac{\partial V}{\partial \theta} \quad (13)$$

However, in order to calculate the sensitivity of the output with respect to the parameters, we must first find the sensitivity of the states with respect to the parameters. We can then combine this with the derivative of the output with respect to the states by using chain rule (14).

$$\frac{\partial y}{\partial \theta} = \frac{\partial x}{\partial \theta}\frac{\partial y}{\partial x} \rightarrow \frac{\partial V}{\partial \theta} = \frac{\partial c_{ss}}{\partial \theta}\frac{\partial V}{\partial c_{ss}} \quad (14)$$

The parameters of interest to be studied are the particle radius $R_s^\pm$ and the electrode thickness $L^\pm$. This results in four separate parameters for both the anode and cathode (15).

$$\theta = \begin{bmatrix}\theta_1^-\\ \theta_2^-\\ \theta_1^+\\ \theta_2^+\end{bmatrix} = \begin{bmatrix}R_s^-\\ L^-\\ R_s^+\\ L^+\end{bmatrix} \quad (15)$$

The first step is to take the derivative of the output equation with respect to the states. This equation is omitted for brevity. As can be noted from (5), the only state that the output voltage is dependent on is c_{ss}^j, which is simply a boundary value of c_s^j.

The second step is to derive the individual sensitivity equations for each parameter. This is done by first evaluating the nominal state equation to determine the nominal solution $x(t,\gamma_0)$, evaluating the Jacobian matrices given by (16), and lastly solving the sensitivity equation (17) for $S(t)$ [11].

$$A(t,\gamma_0) = \frac{\partial f(t,x,\gamma)}{\partial x}\Big|_{x=x(t,\gamma_0),\gamma=\gamma_0}, \quad B(t,\gamma_0) = \frac{\partial f(t,x,\gamma)}{\partial \gamma}\Big|_{x=x(t,\gamma_0),\gamma=\gamma_0} \quad (16)$$

$$\dot{S}(t) = A(t,\gamma_0)S(t) + B(t,\gamma_0), \quad S(t_0) = 0 \quad (17)$$

Therefore, the next step is to derive the sensitivity equations with respect to the states. This is done by taking the derivative of (9)-(12) with respect to θ_i for the appropriate electrodes (18).

$$S_i(t,x,\gamma) = \frac{\partial}{\partial \theta_i}\left[\frac{\partial f(t,x,\gamma)}{\partial x}\right] \quad (18)$$

The sensitivity equations for each parameter with respect to the states can then be computed. The sensitivity equations w.r.t. $\theta_1^- = R_s^-$ are computed as in (19), (20), and (21).

$$S_{1t}^{-}(r,t) = S_{1rr}^{-}(r,t;\theta_0) \tag{19}$$
$$S_{1r}^{-}(0,t) = 0 \tag{20}$$
$$S_{1r}^{-}(1,t) = \frac{1}{D_s^{-} Fa^{-} AL^{-}} I(t) \tag{21}$$

The sensitivity equations w.r.t. $\theta_2^- = L^-$ are computed as in (22), (23), and (24).

$$S_{2t}^{-}(r,t) = S_{2rr}^{-}(r,t;\theta_0) \tag{22}$$
$$S_{2r}^{-}(0,t) = 0 \tag{23}$$
$$S_{2r}^{-}(1,t) = -\frac{R_s^{-}}{D_s^{-} Fa^{-} AL^{-2}} I(t) \tag{24}$$

The sensitivity equations w.r.t. $\theta_1^+ = R_s^+$ are computed as in (25), (26), and (27).

$$S_{1t}^{+}(r,t) = S_{1rr}^{+}(r,t;\theta_0) \tag{25}$$
$$S_{1r}^{+}(0,t) = 0 \tag{26}$$
$$S_{1r}^{+}(1,t) = -\frac{1}{D_s^{+} Fa^{+} AL^{+}} I(t) \tag{27}$$

The sensitivity equations w.r.t. $\theta_2^+ = L^+$ are computed as in (28), (29), and (30).

$$S_{2t}^{+}(r,t) = S_{2rr}^{+}(r,t;\theta_0) \tag{28}$$
$$S_{2r}^{+}(0,t) = 0 \tag{29}$$
$$S_{2r}^{+}(1,t) = \frac{R_s^{+}}{D_s^{+} Fa^{+} AL^{-2}} I(t) \tag{30}$$

With the sensitivity equations derived, we can now solve these four sets of PDEs to compute $S_1^-(r,t)$, $S_2^-(r,t)$, $S_1^+(r,t)$, and $S_2^+(r,t)$.

We are now positioned to apply the chain rule to get the sensitivity of the output with respect to the states. That is, for every parameter, we can now multiply its sensitivity equation by $\frac{\partial V}{\partial c_{ss}}$ to obtain our desired result (31). Note that the sensitivity equations with respect to the state provide the sensitivity evolution with time for all spatial coordinates. The appropriate value of $S_i(r,t)$ to use occurs at the boundary, *i.e.* $S_i(1,t)$.

$$\frac{\partial V}{\partial \theta_i^j} = \frac{\partial V}{\partial c_{ss}^j} \cdot S_i(1,t) \tag{31}$$

The final step is to normalize (31) with respect to each parameter. Without this step, the values provided by the sensitivity vector become skewed by the magnitude of each parameter, making it difficult to perform an objective analysis of each parameter's influence on the output. The normalization is performed by multiplying the final sensitivity vector by the parameter divided by the output (32).

$$\frac{\partial f}{\partial \theta} \cdot \frac{\theta}{f} \rightarrow \frac{\partial V}{\partial \theta_i^j} \cdot \frac{\theta_i^j}{V} = S_i^* \tag{32}$$

The results of (32) can then be gathered in a sensitivity matrix S (33).

$$S = \begin{bmatrix} S_1^{-*} & S_2^{-*} & S_1^{+*} & S_2^{+*} \end{bmatrix} \tag{33}$$

The sensitivity derivation is summarized in Figure 4.

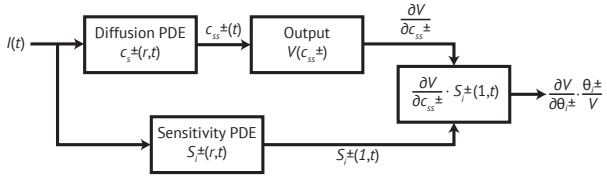

Fig. 4. Block diagram of sensitivity equation derivation. Only the boundary values of $c_s^{\pm}(r,t)$ and $S_i^{\pm}(r,t)$ ($c_s s^{\pm}(r,t)$) and $S_i^{\pm}(1,t)$ are used in the final sensitivity matrix.

D. Sensitivity Analysis

Let $S^T S = D^T C D$. The sensitivity analysis can then be performed by decomposing the matrix $S^T S$ into its constituents C and D. These two matrices are defined as follows (34).

$$D = \begin{bmatrix} \left\|S_1^{-*}\right\| & 0 & 0 & 0 & \\ 0 & \left\|S_2^{-*}\right\| & 0 & & \\ 0 & 0 & \left\|S_1^{+*}\right\| & 0 & 0 \\ 0 & 0 & 0 & \left\|S_2^{+*}\right\| & \end{bmatrix},$$

$$C = \begin{bmatrix} 1 & \frac{\langle S_1^{-*}, S_2^{-*} \rangle}{\|S_1^{-*}\| \|S_2^{-*}\|} & \frac{\langle S_1^{-*}, S_1^{-+*} \rangle}{\|S_1^{-*}\| \|S_1^{+*}\|} & \frac{\langle S_1^{-*}, S_2^{+*} \rangle}{\|S_1^{-*}\| \|S_2^{+*}\|} \\ \frac{\langle S_2^{-*}, S_1^{-*} \rangle}{\|S_2^{-*}\| \|S_1^{-*}\|} & 1 & \frac{\langle S_2^{-*}, S_1^{+*} \rangle}{\|S_2^{-*}\| \|S_1^{+*}\|} & \frac{\langle S_2^{-*}, S_2^{+*} \rangle}{\|S_2^{-*}\| \|S_2^{+*}\|} \\ \frac{\langle S_1^{+*}, S_1^{-*} \rangle}{\|S_1^{+*}\| \|S_1^{-*}\|} & \frac{\langle S_1^{+*}, S_2^{-*} \rangle}{\|S_1^{+*}\| \|S_2^{-*}\|} & 1 & \frac{\langle S_1^{+*}, S_2^{+*} \rangle}{\|S_1^{+*}\| \|S_2^{+*}\|} \\ \frac{\langle S_2^{+*}, S_1^{-*} \rangle}{\|S_2^{+*}\| \|S_1^{-*}\|} & \frac{\langle S_2^{+*}, S_2^{-*} \rangle}{\|S_2^{+*}\| \|S_2^{-*}\|} & \frac{\langle S_2^{+*}, S_1^{+*} \rangle}{\|S_2^{+*}\| \|S_1^{+*}\|} & 1 \end{bmatrix} \tag{34}$$

Matrix D provides a direct quantification of parameter sensitivity with larger numbers indicating higher sensitivity to that parameter. Matrix C provides a measure of linear dependence between parameters. Values close to 1 and -1 indicate that those parameters are very strongly linearly dependent. Values equal to 1 and -1 indicate that the parameters are completely proportional or inversely proportional.

III. Discussion

A. Simulation

The PDEs were discretized for simulation using a combination of second order central finite difference methods and first order forwards and backwards finite difference methods for the boundary conditions. The input current for the system was a pulsed discharge at 0.5C with a 50% duty cycle. All parameter values used were for a $LiCoO_2$ battery due to a lack of comprehensive data for our Zn-MnO_2 system.

Despite the mismatch of parameter values for this simulation, the results are still applicable for any battery system as this sensitivity analysis relates the relative effects of different parameters to each other. While the absolute magnitudes

present in the *D* matrix may not be representative, their relative values are relevant in describing the relationship between chosen parameters.

B. Results

The *D* and *C* matrices for the simulation ran are provided below (35).

$$D = \begin{bmatrix} 14.5850 & 0 & 0 & 0 \\ 0 & 6.8258 & 0 & 0 \\ 0 & 0 & 14.5850 & 0 \\ 0 & 0 & 0 & 6.8258 \end{bmatrix}, \quad C = \begin{bmatrix} 1 & -1 & -1 & 1 \\ -1 & 1 & 1 & -1 \\ -1 & 1 & 1 & -1 \\ 1 & -1 & -1 & 1 \end{bmatrix} \tag{35}$$

Again, for clarification, the parameter vector as in (15) is reproduced below.

$$\theta = \begin{bmatrix} \theta_1^- \\ \theta_2^- \\ \theta_1^+ \\ \theta_2^+ \end{bmatrix} = \begin{bmatrix} R_s^- \\ L^- \\ R_s^+ \\ L^+ \end{bmatrix}$$

The values in *D* indicate that the particle radius is more influential on the output voltage than the electrode thickness for both electrodes. For this particular simulation, this is subject to the parameters used and may change based on different values for D_s^j, α^j, etc.

The more significant result comes from the values present in *C*. The entries corresponding to the linear dependence of particle radius and electrode thickness for each electrode are equal to -1. These values are expected because both parameters only appear in the boundary condition within the sensitivity equations (21), (27), (24), (30). This sensitivity analysis suggests that the particle radius and electrode thickness are inversely proportional to one another.

In reality, this inverse proportionality is not true because the SPM itself assumes that the dynamics occurring at a single particle can be scaled up to represent the entire volume of each electrode. For real batteries, the fraction of each electrode participating in the reaction is limited by electrolyte dynamics, which are assumed away in the SPM, so changes in particle radius cannot be compensated for by changes in electrode thickness and vice versa.

However, this inverse proportionality does reveal that the particle radius and electrode thickness are strongly linearly dependent, even if they are not completely proportional. As a practical point, both parameters should not be changed simultaneously to avoid obfuscating the effects of either on the output voltage.

Ultimately, this analysis yields insight into which parameter should be prioritized for process control during manufacturing. Based on these results for the parameter values used, control of particle size should be prioritized over electrode thickness when seeking to tightly control output voltage.

C. Future Work

Future work should seek to add more insightful parameters that still remain controllable during the manufacturing process. These can include the moles of cycleable zinc $n_{Zn,s}$, the volume fraction of active material ε_s^j, and the specific interfacial surface area α^j. Furthermore, the sensitivities of additional metrics (such as state of charge and cycle life) to these parameters should also be investigated. The SPM itself may need to be augmented by adding back in electrolyte dynamics to more accurately model the true system dynamics [12].

IV. Summary

A parameter sensitivity analysis was performed for battery output voltage with respect to electrode parameters by adapting the single particle model (SPM). The parameters of interest were the particle radius and electrode thickness. Analysis concluded that output voltage is more sensitive to particle radius than electrode thickness and that they are inversely proportional to each other, which is influenced by the simplifying assumptions inherent in the SPM. The results rank the importance of each parameter for use in manufacturing process control.

References

[1] C. C. Ho, J. W. Evans, and P. K. Wright, "Direct write dispenser printing of a zinc microbattery with an ionic liquid gel electrolyte," *Journal of Micromechanics and Microengineering*, vol. 20, no. 10, p. 104009, Sep 2010.

[2] S. J. Moura, M. Krstic, and N. A. Chaturvedi, "Adaptive pde observer for battery soc/soh estimation," *ASME 2012 5th Annual Dynamic Systems and Control Conference joint with the JSME 2012 11th Motion and Vibration Conference*, pp. 101–110, Oct 2012, american Society of Mechanical Engineers.

[3] H. E. Perez and S. J. Moura, "Sensitivity-based interval pde observer for battery soc estimation," *American Control Conference (ACC)*, pp. 323–328, Jul 2015, iEEE.

[4] M. Doyle, T. Fuller, and J. Newman, "Modeling of galvanostatic charge and discharge of the lithium/polymer/insertion cell," *Journal of the Electrochemical Society*, vol. 140, no. 6, pp. 1526–33, Jun 1993.

[5] N. A. Chaturvedi, R. Klein, J. Christensen, J. Ahmed, and A. Kojic, "Algorithms for advanced battery-management systems," *IEEE Control Systems Magazine*, vol. 30, no. 3, pp. 49–68, 2010.

[6] M. Armand and J. M. Tarascon, "Building better batteries," *Nature*, vol. 451, pp. 652–657, 2008.

[7] S. J. Moura, N. Chaturvedi, and M. Krstic, "Pde estimation techniques for advanced battery management systems - part i: Soc estimation," *Proceedings of the 2012 American Control Conference*, Jun 2012, montreal, Canada.

[8] J. P. Tafur, J. Abad, E. Roman, and A. J. F. Romero, "Charge storage mechanism of mno2 cathodes in zn/mno2 batteries using ionic liquid-based gel polymer electrolytes," *Electrochemistry Communications*, vol. 60, pp. 190–194, 2015.

[9] M. Galinski, A. Lewandowski, and I. Stepniak, "Ionic liquids as electrolytes," *Electrochimica Acta*, vol. 51, pp. 5567–5580, 2006.

[10] B. Kim, R. Winslow, I. Lin, K. Gururangan, J. Evans, and P. Wright, "Layer-by-layer fully printed zn-mno2 batteries with improved internal resistance and cycle life," *JoP: Conference Series*, vol. 660, p. 012009, 2015.

[11] H. K. Khalil and J. W. Grizzle, *Nonlinear Systems*. New Jersey: Prentice Hall, 1996.

[12] S. J. Moura, F. Bribiesca Argomeda, R. Klein, A. Mirtabatabaei, and M. Krstic, "Battery state estimation for a single particle model with electrolyte dynamics," *Working Papers*, 2015.